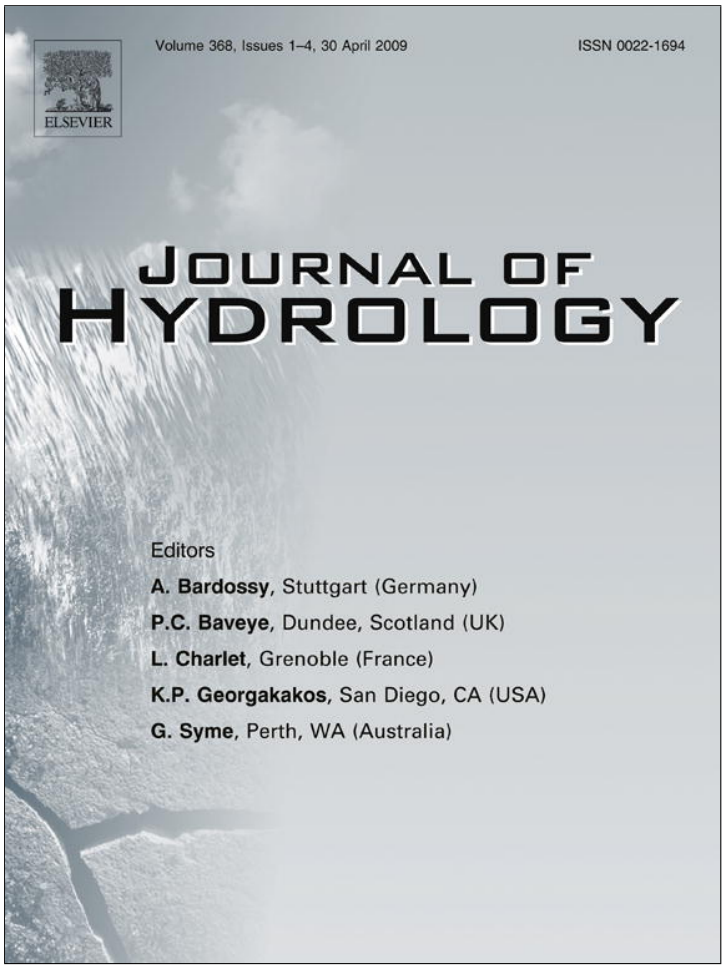

Journal of Hydrology 368 (2009) 131–142

Contents lists available at ScienceDirect

Journal of Hydrology

journal homepage: www.elsevier.com/locate/jhydrol

Long lead-time streamflow forecasting of the North Platte River incorporating oceanic–atmospheric climate variability

Tyrel L. Soukup [a,1], Oubeidillah A. Aziz [b,2], Glenn A. Tootle [b,*], Thomas C. Piechota [c,3], Shaun S. Wulff [d,4]

[a] University of Wyoming, Department of Civil and Architectural Engineering, 1000 East University Avenue, Department 3295, Laramie, WY 82071-2000, United States
[b] University of Tennessee, Department of Civil and Environmental Engineering, 223 Perkins Hall, Knoxville, TN 37996-2010, United States
[c] University of Nevada, Las Vegas, Division of Research and Graduate Studies, Department of Civil and Environmental Engineering, 4505 Maryland Parkway, Box 451087, Las Vegas, NV 89154-1087, United States
[d] University of Wyoming, Department of Statistics, 1000 East University Avenue, Department 3332, Laramie, WY 82071-2000, United States

ARTICLE INFO

Article history:
Received 22 May 2008
Received in revised form 24 October 2008
Accepted 12 November 2008

This manuscript was handled by
K. Georgakakos, Editor-in-Chief, with the assistance of Phillip Arkin, Associate Editor

Keywords:
Singular value decomposition
Sea surface temperatures
500 mbar geopotential height
Streamflow forecast
Exceedance probability

SUMMARY

An evaluation of the influence of oceanic–atmospheric climate variability on streamflow in the upper North Platte River basin is presented. Through the application of Singular Value Decomposition (SVD) statistical methods, sea surface temperatures (SSTs), 500 mbar geopotential height (Z_{500}) values and North Platte streamflow were evaluated over a historical period from 1948 to 2006. This resulted in the identification of new regions of highly correlated SSTs and Z_{500} that may not be represented by existing index regions (Niño 3.4 — defined El Nino Southern Oscillation region, PDO – Pacific Decadal Oscillation, and AMO – Atlantic Multidecadal Oscillation). A long lead-time approach was utilized such that a three month lead-time (seasonal average of monthly SSTs or Z_{500} for October, November, and December) as well as a six month lead-time (seasonal average of monthly SSTs or Z_{500} for July, August, and September) of previous year variability were used as predictors for the following year spring streamflow (seasonal monthly average of April, May, June, and July). Temporal expansion series from SVD were utilized as predictors in a non-parametric model to develop continuous exceedance probability forecasts. The results displayed good skill using SSTs for the six month lead-time forecast and excellent skill using Z_{500} values for the three month lead-time forecast. The improved skill found over basic climatology forecasts will be useful to water managers when trying to predict and manage expected streamflow volumes several months in advance.

Introduction

Over the past several decades, hydrologists and climatologists have developed relationships between large scale oceanic–atmospheric variability and climate (hydroclimatology). Atmospheric – oceanic climatic and sea surface temperature (SST) variability can provide important predictive information about hydrologic variability in regions around the world. Significant research has focused on identifying atmospheric – oceanic climatic phenomena such as the El Niño-Southern Oscillation (ENSO) (Philander, 1990), the Pacific Decadal Oscillation (PDO) (Mantua et al., 1997) and the Atlantic Multidecadal Oscillation (AMO) (Enfield et al., 2001). Further research has identified what influence these phenomena have on US hydrology, including streamflow and snowpack (e.g., Cayan and Peterson, 1989; Cayan and Webb, 1992; Kahya and Dracup, 1993, 1994a,b; Enfield et al., 2001; Rogers and Coleman, 2003; Maurer et al., 2004; McCabe et al., 2004; Tootle et al., 2005; Hunter et al., 2006). The relationships between atmospheric – oceanic climate variability may result in their utilization as long lead-time (e.g., 3–6 months) predictors (forecasters) of various hydrologic responses, including streamflow.

Streamflow forecasting is the process of predicting the volume of water at a specific location for a specific time period. Currently, the Natural Resources Conservation Service (NRCS) and the National Weather Service (NWS) cooperate to generate forecasts around the first of each month between January and June. Nearly all of these forecasts are produced using parametric statistical approaches such as multiple linear regression models (Natural Resources Conservation Service, 2008). An alternative to typical parametric regression techniques is a non-parametric approach.

Non-parametric routines avoid the usual assumption that the data comes from a normal distribution (or any specific distribution). Essentially, a non-parametric model is derived from the data and does not pre-define the form (i.e. linear or non-linear) of the

* Corresponding author. Tel.: +1 865 974 7777; fax: +1 865 974 2669.
E-mail addresses: tlsoukup@gmail.com (T.L. Soukup), oaziz@utk.edu (O.A. Aziz), gtootle@utk.edu (G.A. Tootle), thomas.piechota@unlv.edu (T.C. Piechota), wulff@uwyo.edu (S.S. Wulff).
[1] Tel.: +1 307 766 3299; fax: +1 307 766 2221.
[2] Tel.: +1 865 974 7777; fax: +1 865 974 2669.
[3] Tel.: +1 702 895 4412; fax: +1 702 895 3936.
[4] Tel.: +1 307 766 6483; fax: +1 307 766 3927.

0022-1694/$ - see front matter © 2009 Elsevier B.V. All rights reserved.
doi:10.1016/j.jhydrol.2008.11.047

function. Non-parametric methods have been successfully applied to streamflow forecasting. Lall (1995) performed an extensive analysis of applications of non-parametric probability uses in stochastic hydrology. Several other non-parametric methods (*K* nearest neighbor local polynomials and local weighted polynomials) have been successfully applied to hydrologic (and streamflow) forecasting (Lall and Sharma, 1996; Rajagopalan and Lall, 1999; Souza Filho and Lall, 2003). Piechota and Dracup (1999) applied non-parametric (kernel density estimator) methods to forecasting streamflow for long lead-times and showed significant improvement when comparing the results to the climatology (no skill) forecast (Piechota and Dracup, 1999). The non-parametric kernel density estimator was also successfully applied to El Niño-Southern Oscillation (ENSO) affected streams in eastern Australia and Florida (Piechota et al., 1998; Tootle and Piechota, 2004). The exceedance probability forecast developed provides an example of applying non-parametric techniques to forecasting. An exceedance probability forecast explains the likelihood that a certain streamflow volume will be equaled or exceeded during a certain period of time. Exceedance probability forecasts are used for the design and operation of water resource systems that require a high degree of system reliability (Piechota et al., 2001). However, whether applying parametric or non-parametric techniques (utilizing climate variability), it is vital to identify statistically strong relationships (predictors) between climate variability and streamflow response.

Several methods are typically used to determine the relationship between two spatial–temporal arrays of data such as climate variability (e.g., SSTs) and streamflow. Common methods include correlation analysis, principal component analysis and singular value decomposition (SVD). Bretherton et al. (1992) evaluated several statistical methods and concluded SVD was simple to perform and preferable for general use. In a study between wintertime sea surface temperature and 500 mbar height (Z_{500}) anomalies, Wallace et al. (1992) determined that SVD isolates the most important modes of variability as well as discovering a coupling between the interannual variability of SST and Z_{500} due to their common link with global wave patterns. SVD has been used to identify relationships between oceanic SST variability and hydrologic variability. Wang and Ting (2000) evaluated Pacific Ocean SSTs and continental US precipitation for concurrent (overlapping) time periods and identified simultaneous patterns of SST influence on precipitation. Uvo et al. (1998) applied SVD to evaluate Pacific and Atlantic Ocean SSTs (independently) and northeast Brazilian precipitation utilizing both a simultaneous and lagged approach. Rajagopalan et al. (2000) utilized SVD and applied a lag approach to evaluate global SST impacts on continental US drought. Shabbar and Skinner (2004) applied SVD and utilized a lag approach in which winter global SSTs and summer Canadian drought [e.g., Palmer Drought Severity Index (PDSI) values] were evaluated and determined, with each mode representing a distinct oceanic/atmospheric phenomena (e.g., 1st mode – AMO, 2nd mode – ENSO, 3rd mode – PDO). Tootle and Piechota (2006) analyzed Pacific and Atlantic Ocean SSTs which resulted in the identification of several SST regions associated with streamflow regions in the continental United States. Tootle et al. (2008) applied this approach (SVD) to Pacific and Atlantic SSTs and Colombia streamflow, identifying several SST and streamflow regions of significance.

When examining the impacts of oceanic–atmospheric climate variability, a significant influence on that variability comes from various dynamics at different pressure levels in the atmosphere. In order to reference the height of the various pressure regimes, the term geopotential height is used. In essence, geopotential height is the height to the pressure zone of interest, as measured above the mean sea surface elevation. Blackmon (1976) did a study of the 500 mbar geopotential height (Z_{500}) of the northern hemisphere which presented long term averages of atmospheric parameters. Through a comparison, described in the study, interannual variability can be obtained and would allow for a comparison of various data sets and thus generate a circulation model that has the ability to replicate the atmosphere's behavior in low to mid frequency domains and in various spatial scales. Building upon the 1976 study, Blackmon et al. (1977) explored the behavior of the 500 mbar wind statistics upon northern hemisphere wintertime circulation. The results of these studies suggested that Z_{500} index values can be attributed to substantial impacts on climate. On a global level Xoplaki et al. (2000) determined that the link between precipitation over Greece and changes in large scale atmospheric circulation are strong, specifically in relation to 500 mbar geopotential heights. As related to the work of this paper, Serreze et al. (1998) evaluated the relationship between snowfall and low frequency atmospheric variability and found that the troughs and ridges associated with the 500 mbar zone do play a role in the characteristics of snowfall over the eastern United States. Grantz et al. (2005) explored the impacts of including Z_{500} height index values as predictors in streamflow forecasting models and discovered an improved skill with such an addition.

The North Platte River (Fig. 1) originates in north central Colorado with tributaries and contributing basins predominately located in mountainous regions of Colorado and Wyoming. As a result, most of the annual streamflow can be attributed to melting snowpack that has accumulated during the winter and early spring months in the mountainous headwater regions. The North Platte River flows north into Wyoming, then east to Nebraska. Present and future use of water resources in the North Platte River Basin (NPRB) are heavily regulated and controlled by the Supreme Court Decree for the North Platte River (North Platte River Basin Overview, 2008). Recent lawsuits regarding interstate water allocations have augmented the need for a more skillful and longer lead-time forecast. Currently, only parametric (regression) models are used to develop a relationship between predictor variables (precipitation, snow water equivalent, antecedent streamflow, etc.) and the predictand (April–May–June–July streamflow volume). From a forecasting perspective, the challenge with the NPRB is the lack of a distinct climate signal (e.g. ENSO, PDO, AMO) per research performed on unimpaired streamflow and snowpack in the continental and western US (Tootle et al., 2005; Hunter et al., 2006).

The proposed research will develop a unique long lead-time (3–6 months) streamflow forecast of unimpaired streamflow stations in the NPRB utilizing oceanic–atmospheric climate information. Similar to Grantz et al. (2005), Pacific and Atlantic Ocean SST variability and Z_{500} index values will be utilized as predictors. However, in lieu of using correlation to identify predictors, SVD techniques will be applied to identify spatial regions of SSTs and Z_{500} that relate to streamflow variability in the NPRB. Additionally, a non-parametric approach will be utilized to develop an exceedance probability streamflow forecast comparable to the work of Piechota et al. (2001).

Data

Streamflow data

Data from four unimpaired streamflow stations (Q1 – #06620000, Q2 – #06625000, Q3 – #06630000 and Q4 – #06635000) in the Upper North Platte River Basin (Fig. 1) were obtained from the US Geological Survey (USGS) National Water Information System (United States Geological Survey, 2007). USGS provides historical monthly mean streamflow in cubic feet per second (cfs). The average monthly streamflow rate in cfs for April, May, June and July (AMJJ) were summed and converted into

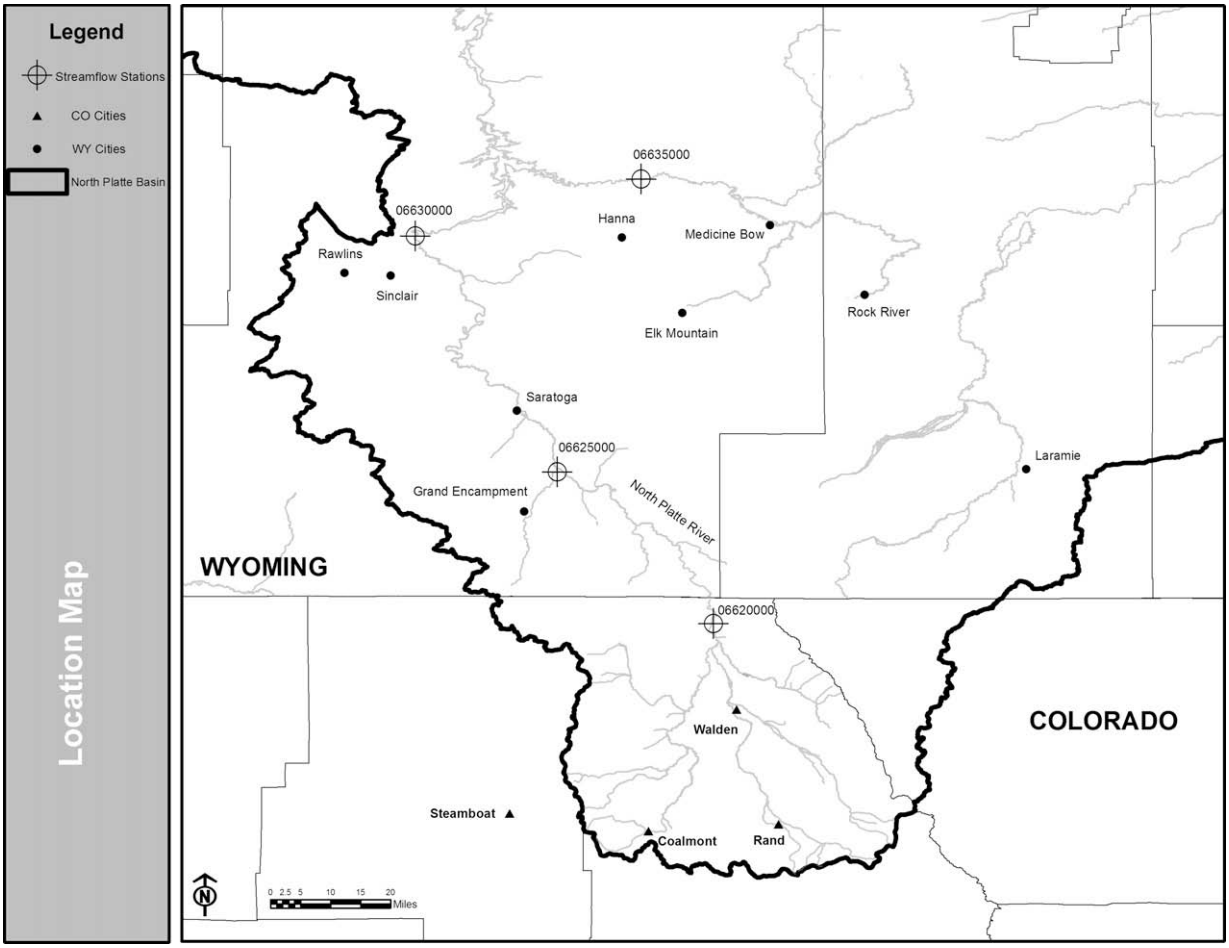

Fig. 1. North Platte River Basin and USGS streamflow stations location map.

streamflow volumes using appropriate conversions. The period of streamflow volume used in the analysis was 1949–2006 (57 years).

Climatic indices

Three of the applicable predefined datasets representing oceanic–atmospheric climatic phenomena are the Niño 3.4 index, the PDO index and the AMO index. The average monthly values for the climatic indices (Niño 3.4, PDO and AMO) were averaged for the six month lead-time period of July, August and September [JAS(-1)] as well as for the three month lead-time period of October, November and December [OND(-1)]. The (-1) nomenclature identifies that the predictor periods are for the previous year to the predictand, AMJJ streamflow. The time span averaged was 1948–2005 (57 years) and preceded the streamflow volumes used by one year.

The Niño 3.4 (Trenberth, 1997) SST region is located along the equatorial Pacific Ocean (5°S–5°N, 170°–120°W) and monthly index data were obtained from the NOAA ESRL Physical Sciences Division (http://www.cdc.noaa.gov/Pressure/Timeseries/Nino34/). The Niño 3.4 index was used since it is an overall representation of ENSO. The PDO is a oceanic/atmospheric phenomena associated with persistent, bimodal climate patterns in the northern Pacific Ocean (poleward of 20° north) that oscillate with a characteristic period on the order of 50 years (a particular phase of the PDO will typically persist for about 25 years) (Mantua et al., 1997; Mantua and Hare, 2002). PDO Index (Mantua et al., 1997; Hare and Mantua, 2000) values were obtained from the Joint Institute for the Study of the Atmosphere and Ocean, University of Washington (http://tao.atmos.washington.edu/pdo/). The Atlantic Multidecadal Oscillation (AMO) index was introduced by Enfield et al. (2001) as a simple basin average of North Atlantic Ocean (0–70°) sea surface temperatures (SSTs). The AMO index consists of detrended (dividing, centering and re-scaling the data to account for unimodal data sets) SST anomalies for the previously defined Atlantic Ocean region. AMO index values are available from the National Oceanic and Atmospheric Administration (NOAA) ESRL Physical Sciences Division (http://www.cdc.noaa.gov/Pressure/Timeseries/).

Pacific and Atlantic ocean sea surface temperature data

SST data for the Pacific and Atlantic Oceans were obtained from the National Climatic Data Center (http://www.cdc.noaa.gov/cdc/data.noaa.ersst.html). The oceanic SST data consists of average monthly values for a 2° by 2° grid cell (Smith and Reynolds, 2004). The extended reconstructed global SSTs were based on the Comprehensive Ocean–Atmosphere Data Set (COADS) from 1854 to present (Smith and Reynolds, 2003).

The overall gridded data region of Pacific Ocean SST data used for the analysis was longitude 100°E–80°W and latitude 30°S–60°N while the region of Atlantic Ocean SST data used for the analysis was longitude 80°W–20°W and latitude 30 S–60°N. The longitudinal boundaries of this study (100°E–20°W) extended the regions of Grantz et al. (2005) (100°E–60°W) to encompass the possibility of more Atlantic ocean influences while the latitudinal boundaries were identical. Similar regions were explored by Tootle

and Piechota (2006) due to these regions representing the majority of oceanic–atmospheric climate influences on US climate (i.e., storm tracks such as Pacific Ocean frontal storms). The regions selected were also similar to other studies, such as those of Wang and Ting (2000). Similar to the climate indices, average monthly values were averaged for the predictor seasons [JAS(-1) and OND(-1)] for each SST cell.

500 mbar Geopotential height index data (Z_{500})

The monthly Z_{500} index data are a product of the NCEP/NCAR Reanalysis 40-year Project (Kalnay et al., 1996) and can be obtained from the NOAA Physical Sciences Center (http://www.cdc.noaa.gov/cgi-bin/Composites/printpage.pl). The Z_{500} index data are given on a $2.5^\circ \times 2.5^\circ$ latitude and longitude grid and are available from 1948 to 2008. The overall gridded data region of data used for the analysis was longitude 100°E–20°W and latitude 30°S–60°N, similar to the previously described SST regions. Like the SSTs, average monthly values were averaged for the predictor seasons [JAS(-1) and OND(-1)] for each Z_{500} cell.

Methods

Climate/streamflow relationships

Comparable to Grantz et al. (2005), the first step was to analyze relationships between potential predictors and predicants. The relationship between ocean-atmospheric variability and streamflow was examined through the development of a correlation table. The correlation table was created using typical correlation techniques between the seasonal [JAS(-1) and OND(-1)] climate indices (Niño 3.4, PDO and AMO) and the four streamflow (AMJJ) stations (Q1, Q2, Q3, Q4).

Singular value decomposition (SVD)

Grantz et al. (2005) examined the relationships between streamflow and oceanic–atmospheric signals using visual inspection of correlation maps and composite analyses. The work presented here builds upon that methodology through the use of SVD. SVD is a powerful statistical tool for identifying coupled relationships between two, spatial–temporal fields. Bretherton et al. (1992) provides a detailed discussion of the theory of SVD, while Tootle et al. (2008) and Tootle and Piechota (2006) provide a brief description of SVD, as applied in the current research.

Initially, a matrix of standardized SST (or Z_{500}) anomalies and a matrix of standardized streamflow anomalies (for the four NPRB stations) were developed. The time dimension of each matrix (i.e., 57 years) must be equal while the spatial component (i.e., SST cells or Z_{500} and North Platte streamflow stations) can vary in dimension. The cross-covariance matrix was then computed for the two spatial, temporal matrices and SVD was applied to the cross-covariance matrix and physical information regarding the relationship between the two was obtained. The resulting SVD of the cross-covariance matrix created two matrices of singular vectors and one matrix of singular values. The singular values were ordered such that the first singular value (1st mode) was greater than the second singular value and so on. Bretherton et al. (1992) defines the squared covariance fraction (SCF) as a useful measurement for comparing the relative importance of modes in the decomposition. Each singular value was squared and divided by the sum of all the squared singular values to produce a fraction (or percentage) of squared covariance for each mode.

Finally, the two matrices of singular vectors were examined, generally referred to as the left (i.e., SST or Z_{500}) matrix and the right (i.e., streamflow) matrix. The first column of the left matrix (1st mode) was projected onto the standardized SST or Z_{500} anomalies matrix and the first column of the right matrix (1st mode) was projected onto the standardized streamflow anomalies matrix. This resulted in the 1st temporal expansion series of the left and right fields, respectively. The left heterogeneous correlation figure (for the 1st mode) was determined by correlating the SST or Z_{500} values of the left matrix with 1st temporal expansion series of the right field and the right heterogeneous correlation figure (for the 1st mode) was determined by correlating the streamflow values of the right matrix with the 1st temporal expansion series of the left field. The left temporal expansion series have a physical meaning since they represent SST or Z_{500} variability that may not already be included in existing SST indices and could represent a new index of SST variability. This may then be useful in forecasting streamflow for stations that have high correlations with the temporal expansion series. Utilizing an approach similar to Rajagopalan et al. (2000) and Uvo et al. (1998), heterogeneous correlation figures displaying 90% significant correlation values for SST and Z_{500} regions were reported. These reported correlations statistically differ from zero at a 10% significance level. A 10% significance level was selected to balance the need to identify correlations that differ from zero, while also recognizing that the relationships between SSTs and Z_{500} is subtle. As a result, correlations which are large in magnitude may not be detected at smaller significance level (e.g., 1%). While SVD is a powerful tool for the statistical analysis of two spatial, temporal fields, there exist several limitations to its use that should be investigated (Newman and Sardeshmukh, 1995). Generally, if the leading (1st, 2nd and 3rd) modes explain a significant amount of the variance of the two fields, then SVD can be applied to determine the strength of the coupled variability present (Newman and Sardeshmukh, 1995). However, when using SVD to examine two fields, the examiner must exhibit caution when attempting to explain the physical cause of the results (Newman and Sardeshmukh, 1995).

Forecast methodology

The streamflow forecast developed is a continuous exceedance probability curve that can be used for any assumed risk level and was developed by Piechota et al. (2001). The "no skill/climatology" forecast curve is generated by dividing the rank of each historical value by the total number of years in the record.

Two advantages are found using the model developed by Piechota et al. (2001): it considers the continuous relationship between the predictand and the predictor, and it does not assume a particular model structure. It suffers, however, from its semi-empiricism; fitting the model to the data points assumes that the historical data represents the entire population. A detailed description of the methodology and model can be found in Piechota et al. (2001) and Piechota et al. (1998). A brief description of the model (for one predictor) is provided below:

1. The climate predictor values (P_i) for each year and the corresponding streamflow predictand values (Q_i) for each year are compiled, where (P_i) represents the temporal expansion series obtained from SVD, as described in the methods section, for SSTs or Z_{500} index values.
2. The streamflow values (Q_i) are ranked in ascending order and the corresponding climate predictor (P_i) for the corresponding year of the streamflow are noted.
3. The first data point for analysis occurs immediately after the five lowest streamflow values (Q_i) and the last point for analysis occurs immediately prior to the five highest streamflow values (Q_i). This is required since a minimum of five values are needed to generate a probability density function.

4. The first data point for analysis is the sixth ranked streamflow value (lowest to highest) based on #3 above. Using the kernel density estimator (Silverman, 1986; Piechota et al., 1998), a probability density function is developed for all climate predictor values below the first data point and a probability function is developed for all climate predictor values above the first data point. Whereas $f(x)$ is the probability density function expressed as,

$$f(x) = \frac{1}{hn}\sum_{i=1}^{n}\left(\frac{x - x_i}{h}\right)$$

$$h_i = 0.9A_i n_i^{-\left(\frac{1}{5}\right)}$$

$$A_i = \min\left(\sigma_i, \frac{\text{interquartile range}}{1.34}\right)$$

where X_1 to X_i is a set of n observations, $k()$ is the kernel function, h is the bandwith, optimal $h = h_i$, σ_i is the stdev of predictor data in each subset i, and n_i is the # of observations in each subset, and the Bayes probability theorem is expressed as,

$$\text{Prob}\left(\frac{Q_i}{x}\right) = \frac{P_i f_i(x)}{\sum_{i=1} k P_i f_i(x)}$$

where X is the predictor value, Q_i is the streamflow, P_i is the prior probability streamflow, and $f_i(x)$ is the probability density function of prior X value.

5. A unique probability value is determined for each predictor value, given the sixth ranked streamflow value. These values are single points on the exceedance probability curve (probability versus streamflow). The procedure is then repeated for the seventh ranked streamflow value and so on.
6. An exceedance probability is then determined for each predictor value. The forecast curve will represent the probability of exceeding a value of streamflow, based on the value of the predictor.
7. The final exceedance probability forecast is found by combining the three individual forecasts into one combination forecast that has better overall skill. The combination forecast is found by applying weights a, b, and c to the three models so that the weights add up to one. The optimal forecast is found by applying more weight to individual forecasts that better predicts streamflow and less weight to poor individual forecasts. These optimal weights are determined by an optimization procedure that evaluates the Linear Error in Probability Space (LEPS) score for all possible combinations, using weighting increments of 0.02 in which the weights vary between 0 and 1 for each model. The final combination forecast is the model with the highest LEPS score.

The skill of the forecast, as produced by the model, was measured using the Linear Error in Probability Space (LEPS) score. The LEPS score is a measure of skill that was originally developed to assess the position of the forecast and the position of the observed values in the cumulative probability distribution (non-exceedance probability); the LEPS score can be used for continuous and categorical variables (Ward and Folland, 1991; Potts et al., 1996). A modified LEPS score is required due to the absence of a convenient measure of skill for an exceedance probability forecast. A better measure of skill is one in which more weight is given to a forecast that effectively predicts low or high flow and less weight to a forecast that successfully predicts average flow. The application of the LEPS score is desirable here because it is less sensitive to changes near the center of the cumulative probability distribution and more sensitive to forecasts of high or low values. Essentially, it rewards a successful forecast of extreme values (Piechota et al., 2001). The developmental steps and the equations used to generate a LEPS score for an exceedance probability forecast can be reviewed in Piechota et al. (2001) and a brief description is hereby provided. In terms of probability, the LEPS score measures the distance between the forecast and observed values. First, a "no skill" or "climatology" curve was developed for the observed yearly streamflow values. The "climatology" curve was created by ranking observed yearly streamflow values in decreasing order (i.e., exceedance probability) of magnitude and dividing the rank of each observed value by the total number of years in the record. The LEPS score is defined as

$$S'' = 3^*(1 - |\text{Pf} - \text{Po}| = \text{Pf2} - \text{Pf} + \text{Po2} - \text{Po}) - 1$$

where Pf and Po are the forecasted and observed cumulative probabilities, respectively. The LEPS score was calculated for each year and "good" or "bad" forecast years were identified. The average skill (SK) is defined as

$$SK = \frac{\sum 100S''}{\sum S''_m}$$

where the summation S'' is for all years of record. If S'' is positive, $S''m$ is the sum of the best possible forecast (i.e. Pf = Po) for all years of record. If S'' is negative, $S''m$ is the sum of the worst possible forecast (i.e. Pf = 1 or 0) for all years of record. A LEPS SK score of greater than +10% is generally considered good skill.

The skill associated with each individual forecast is calculated for calibration and cross-validation analyses. The LEPS score for the calibration analysis does not provide an independent skill score because it is based on the same data in which the model was calibrated. To report the skill scores explained in the results section, each individual yearly calibrated and cross-validated LEPS skill score was averaged over the entire 57 year period of record to develop an overall average forecast skill. Additionally, various combinations of different predictors (i.e. AMO, SST1, 500 mb1, Niño 3.4, SST1, 500 mb1) were modeled in an attempt to obtain an optimal weight amongst the various predictors.

Results

Climate indices

As shown in Table 1, and as similarly reported by Grantz et al. (2005), the standard indices did not show significant relationships with spring streamflow volumes at any of the locations. Consequently, as described by Grantz et al. (2005), an investigation between large scale oceanic–atmospheric variability and its link with streamflow was examined as a potential predictor.

When correlating the PDO index with the four previously defined streamflow stations (AMJJ volume) for both three and six month [JAS(-1)] lead-times, the correlation values resulted in no stations exceeding 90% significance. Similarly, the Niño 3.4 index resulted in none of the four stations exceeding 90% significance for either time period. The Niño 3.4 and PDO correlation coefficient values for both JAS(-1) and OND(-1) for Q1, Q2, Q3 and Q4 are close to 0 and therefore conclude that the Niño 3.4 and PDO signals are not prominent in the upper NPRB. When correlating the AMO index, all four stations exceeded 90% significance for the JAS(-1) (six month) lead-time period, whereas only one exceeded 90% significance for the three month lead-time. The AMO displays a stronger presence in the NPRB, as shown by its higher correlation coefficient values; however the coefficient values are not strong enough to form the basis for a skillful forecast. The correlation analysis was a preliminary study which verified the need to generate regions through the use of

Table 1
Correlation table of current seasonal (spring–summer, AMJJ) streamflow (Q) and previous [JAS (-1) and OND(-1)] seasonal climate indices (Nino 3.4, PDO, AMO) and Temporal Expansion Series (1st, 2nd, and 3rd modes) for SSTs[1, 2, and 3] and Z_{500} [1, 2, and 3].

JAS(-1)	Q1 (AMJJ)	Q2 (AMJJ)	Q3 (AMJJ)	Q4 (AMJJ)	OND(-1)	Q1 (AMJJ)	Q2 (AMJJ)	Q3 (AMJJ)	Q4 (AMJJ)
Nino 3.4	−0.03	−0.07	0.02	0.17	Nino 3.4	−0.04	−0.09	0	0.19
PDO	0.02	−0.03	−0.04	0.04	PDO	−0.12	−0.15	−0.15	−0.01
AMO	−0.24	−0.25	−0.27	−0.37	AMO	−0.17	−0.15	−0.16	−0.34
SST1	0.43	0.41	0.49	0.54	SST1	0.52	0.49	0.53	0.58
SST2	−0.09	−0.16	−0.06	0.25	SST2	−0.09	−0.16	−0.04	0.25
SST3	0.09	0.07	−0.17	0.03	SST3	0.17	−.06	−0.11	−0.00
500 mb1	0.38	0.42	0.43	0.38	500 mb1	0.52	0.53	0.56	0.45
500 mb2	−0.05	−0.04	−0.06	0.16	500 mb2	−0.02	−0.05	−0.06	0.16
500 mb3	0.03	−0.10	0.06	0.00	500 mb3	0.15	−0.11	−0.02	−0.02

SVD that showed a significant relationship to the NPRB. Additionally, each predefined climate index was analyzed through the forecast model such that calibration and cross-validation skill was reported. As explained by Tootle and Piechota (2004), calibration uses all of the data to calibrate the weights and then computes the skill based on all the data. Table 2 shows the weights (in percentage) applied by the cross-validation model to each index. The calibration and cross-validated skill score, also in percentage, are displayed immediately below the weights values. The weights displayed show that for JAS(-1), 100% of the weight to develop the cross-validated exceedance probability forecast was applied to the AMO signal. The LEPS scores for the calibration analysis were greater than +10% for Q2 and Q4. However, cross-validation provides a more independent assessment of the forecast skill and of the weights applied to each model (Elsner and Schmertmann, 1994; Michaelsen, 1987). Cross-validation allows the model to remove a year, calibrate the model, and then test the model on the year that was removed. This procedure is repeated for all years. The use of cross-validation eliminates spurious predictors and artificial skill. The LEPS score for the cross-validation analyses drops considerably when compared to the LEPS score for the calibration analysis. It can be reasoned that a good forecast would be indicated by a cross-validated LEPS score at or above +10%, which is not evident in any of the climate index results. The highest cross-validated skill score for the JAS(-1) was the model run with Q4 and the AMO index, resulting in a value of 1.4%. The results of the OND(-1) run exhibit different behavior in terms of the weights being split amongst different signals. The Q1 run resulted in 33% of the forecast weight being placed on the Niño 3.4 signal. Different weights are selected by the model in an attempt and achieve the most skillful forecast. The weights selected by the model for each run are shown in Table 2. The calibration scores are all below +10% as well as all of the cross-validated LEPS score values being negative, indicating the climate indices for the OND(-1) are poor predictors of streamflow volume in the NPRB.

Sea surface temperatures (SSTs)

When applying SVD to Pacific/Atlantic Ocean SSTs and North Platte streamflow, this resulted in squared covariance fractions (SCF) of 84.3% – 1st mode, 12.7% – 2nd mode and 1.7% – 3rd mode for the JAS(-1) lead-time period. The OND(-1) lead-time period resulted in SCFs of 81.2% – 1st mode, 15.3% – 2nd mode and 2.0% – 3rd mode. Therefore, for both lead-times, the 1st mode clearly identifies the strongest relationships. The total number of Pacific/Atlantic Ocean SST cells was 4329. For the 1st mode of JAS(-1) variability, 528 Pacific/Atlantic Ocean SST Cells (12.2%) were identified as significant. Fig. 2 represents heterogeneous correlation maps (90% significance or $|r| > 0.21$) displaying significant Pacific/Atlantic Ocean SST for the 1st mode of SVD for the JAS(-1) lead-time. All four North Platte River streamflow stations were identified as being significant. For the 1st mode of OND(-1) variability, 493 Pacific/Atlantic Ocean SST Cells (11.4%) were identified as significant. Modes 2 and 3 were not reported based on the lack of significance of the SCF for both lead-times.

The results of the forecast model runs for JAS(-1) and OND(-1) are presented in Table 2. The table displays the temporal expansion series as row headings, for modes 1, 2 and 3 (SST1, SST2 and SST3, respectively) of the SVD analysis, on the left. The weights applied to each temporal expansion series are displayed as a percentage, for the respective streamflow station (Q1, Q2, Q3 and Q4). The model applied 100% of the weight of the forecast on the first mode temporal expansion series (SST1). The 100% weighting acknowledges that the region defined through the SVD analysis for mode 1 has the strongest spatial–temporal relationship [84.3% – JAS(-1) and 81.2% – OND(-1)] and consequently is the best predictor for

Table 2
Weighting and LEPS [Calibration (Cal) and Cross-Validation (CV)] score skill table of current seasonal (spring–summer, AMJJ) streamflow (Q) and previous [JAS (-1) and OND(-1)] seasonal climate indices (Nino 3.4, PDO, AMO) and Temporal Expansion Series (1st, 2nd, and 3rd modes) for SSTs[1, 2, and 3] and Z_{500} [1, 2, and 3].

JAS(-1)	Q1 (AMJJ) (%)	Q2 (AMJJ) (%)	Q3 (AMJJ) (%)	Q4 (AMJJ) (%)	OND(-1)	Q1 (AMJJ) (%)	Q2 (AMJJ) (%)	Q3 (AMJJ) (%)	Q4 (AMJJ) (%)
Nino 3.4	0	0	0	0	Nino 3.4	33	95	77	0
PDO	0	0	0	0	PDO	0	0	3	2
AMO	100	100	100	100	AMO	67	5	20	98
Cal skill	9.2	11.6	8.9	13.8	Cal skill	5.0	6.1	5.2	8.8
CV skill	1.0	0.7	−1.4	1.4	CV skill	−8.6	−4.5	−9.6	−0.7
SST1	100	100	100	100	SST1	100	100	100	100
SST2	0	0	0	0	SST2	0	0	0	0
SST3	0	0	0	0	SST3	0	0	0	0
Cal skill	16.4	21.4	18.2	20.6	Cal skill	16.5	21.4	18.1	16.6
CV skill	7.3	8.5	8.1	10.2	CV skill	2.9	6.2	5.7	4.7
500 mb1	100	100	100	100	500 mb1	100	100	100	100
500 mb2	0	0	0	0	500 mb2	0	0	0	0
500 mb3	0	0	0	0	500 mb3	0	0	0	0
Cal skill	16.7	15.4	15.3	14.3	Cal skill	23.9	25.1	25.0	20.3
CV skill	3.6	3.3	5.7	4.5	CV skill	12.8	14.6	13.7	10.4

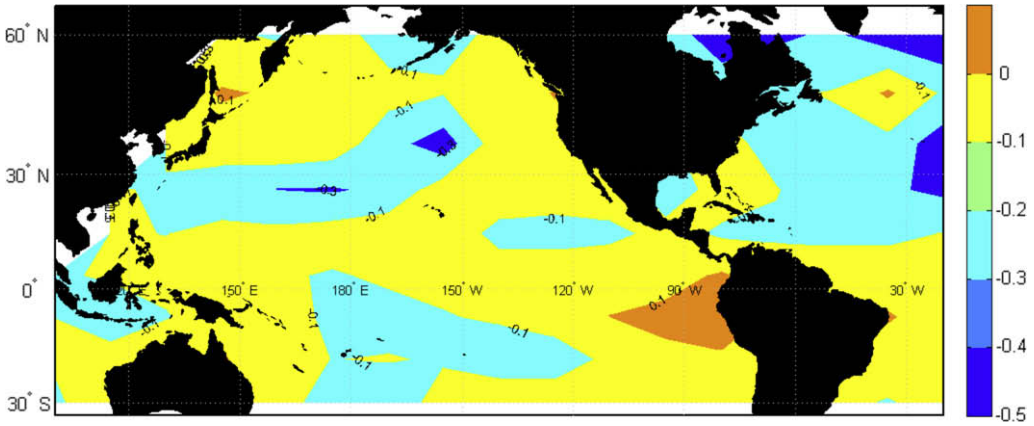

Fig. 2. Heterogeneous correlation map showing significant [$|r| > 0.21$ for 90% ($p < 0.1$) significance threshold] SST regions as related to NPRB streamflow stations for JAS(-1) six month lead-time.

all four streamflow stations. The calibration and cross-validated LEPS skill scores displayed in Table 2 are averages over the entire period of analysis (57 years). The six month lead-time [JAS(-1)] calibration LEPS skill scores are all above +10%. Even more appealing are the results of the JAS(-1) cross-validated LEPS skill scores. Three of the four stations exhibit a cross-validated skill score near +10% with Q4 actually surpassing +10% with a value of +10.2%. For the three month lead-time forecast [OND(-1)], the calibrated skill scores were close to those of the six month lead-time scores. However, the cross-validated skill scores show a general decrease in skill value, with the most skillful result being +6.2% for Q2. It should be noted that for both lead-time periods, the cross-validated skill for all analyses are above zero, indicating that the forecast model has better skill than the climatology forecast (skill = 0). Fig. 3 presents examples of poor and good exceedance probability forecasts for individual years for each streamflow station for the JAS(-1) lead-time. For example, the 1963 Q2 vs. JAS SST represents a good forecast (cross-validated LEPS score of 61.17%). Using this graph, a water manager, assuming a 50% risk level (50% exceedance) would have correctly projected an average AMJJ streamflow volume of 1.12×10^8 cubic meters (m^3). Utilizing the climatology forecast at a 50% exceedance level, the water manager would have over-forecasted the projected supply at $1.75 \times 10^8\ m^3$. On the same note, there are risks associated with poor forecasts. Using the 1996 Q1 vs. JAS SST graph as an example of a poor forecast (cross-validated LEPS score of −61.08%), a water manager assuming a 50% risk (50% exceedance) would have predicted a streamflow volume of $2.01 \times 10^8\ m^3$ when in fact $4.69 \times 10^8\ m^3$ was actually reported. Nevertheless, by averaging the entire period of record (57 years), for each streamflow station, the positive cross-validated skill score is relatively close to +10%. This provides evidence for a greater number of good forecasts than poor forecasts.

500 mbar Geopotential height index

SVD analysis of 500 mbar Geopotential Height Index values and North Platte streamflow resulted in squared covariance fractions (SCF) of 70.3% – 1st mode, 24.1% – 2nd mode and 3.4% – 3rd mode for the JAS(-1) lead-time. SCFs for the OND(-1) lead-time were 73.4% – 1st mode, 22.0% – 2nd mode and 2.5% – 3rd mode. The 1st mode of variability (only) was reported, based on the significant squared covariance fraction reported for the 1st mode. The total number of Z_{500} Cells was 3589. For the 1st mode of variability and the JAS period, 94 Z_{500} Cells (2.6%) were identified as significant. For the 1st mode of variability and the OND(-1) period, 207 Z_{500} Cells (5.8%) were identified as significant. OND(-1) heterogeneous correlation maps (90% significance or $|r| > 0.21$) displaying significant Z_{500} regions and North Platte River streamflow stations for the 1st mode of SVD are shown in Fig. 4.

Table 2 displays the results of the model weights, calibration and cross-validation skill scores, in the same format as described in the SST results section. Similar to the SST results, the temporal expansion series for mode 1 of Z_{500} turned out to be the predominant predictor driving the model. One hundred percent (100%) of the weight was applied to 500 mb1 for both lead-times at all streamflow stations. Interestingly, we find that for both three and six month lead-times, the calibration skill values are all above +10% with substantial increase in skill for the three month OND(-1) lead-time. Likewise an improvement in cross-validated skill is noticed for the OND(-1) lead-time over the JAS(-1) period. The cross-validated skill scores for the OND(-1) lead-time all exceed +10% whereas only one of the JAS(-1) skill scores exceed +5%. An explanation for these results will be examined in the discussion section. These results were similar to those of Grantz et al. (2005) in that an increase in skill was shown with decreasing lead-time when using the Z_{500} index as a predictor. Examples of poor and good exceedance probability forecasts utilizing Z_{500} are presented in Fig. 5. Please refer to the discussion in the SST results section regarding the interpretation of poor and good exceedance probability forecast graphs.

Discussion

The predefined climate index regions for the Niño 3.4, PDO and AMO lack the spatial–temporal relationship needed to produce skillful forecasts for the NPRB. In an attempt to find an ideal relationship, we expanded upon the methods of Grantz et al. (2005). Through the use of a more powerful spatial–temporal analysis (SVD) we were able to locate "significant regions" of SST and Z_{500} regions that tele-connected with the streamflow stations in the NPRB. The correlation values resulting from the SVD analysis, for each predictor, are displayed in Table 1. The SST "significant region" determined in this study was similar to that identified by Wang and Ting (2000), Tootle and Piechota (2006) and Grantz et al. (2005). The unique aspect about the NPRB is that no significant SST regions were identified in the vicinity of the traditional ENSO belt (equatorial Pacific Ocean region). The predominant "significant region" identified for SSTs in this study was located approximately 20°W and 25° N of the Niño 3.4 region. Likewise, no significant regions were identified in the neighborhood of the typical PDO region. These findings verify the initial analysis which resulted in poor correlation values between the Nino 3.4, PDO and NPRB streamflow stations.

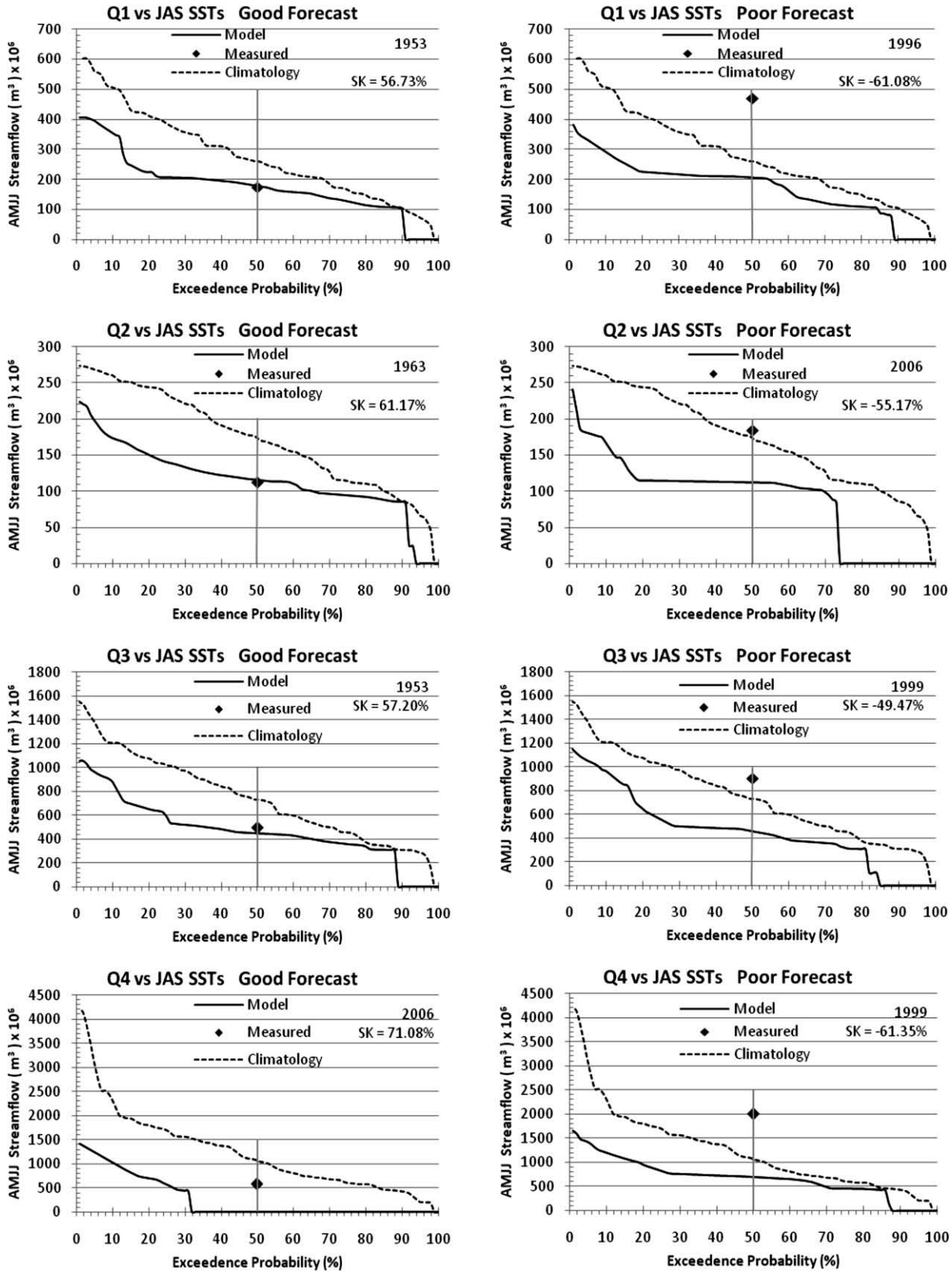

Fig. 3. Examples of poor and good forecasts for JAS(-1) SSTs and individual streamflow stations.

As a result of the stronger correlation values between NPRB streamflow stations and the AMO index in the preliminary analysis, the east longitudinal boundary was extended in an attempt to capture more Atlantic Ocean SST variability. The majority of the Atlantic Ocean SSTs displayed a significant relationship to NPRB streamflow (Fig. 2), with a region off the coast of Africa dis-

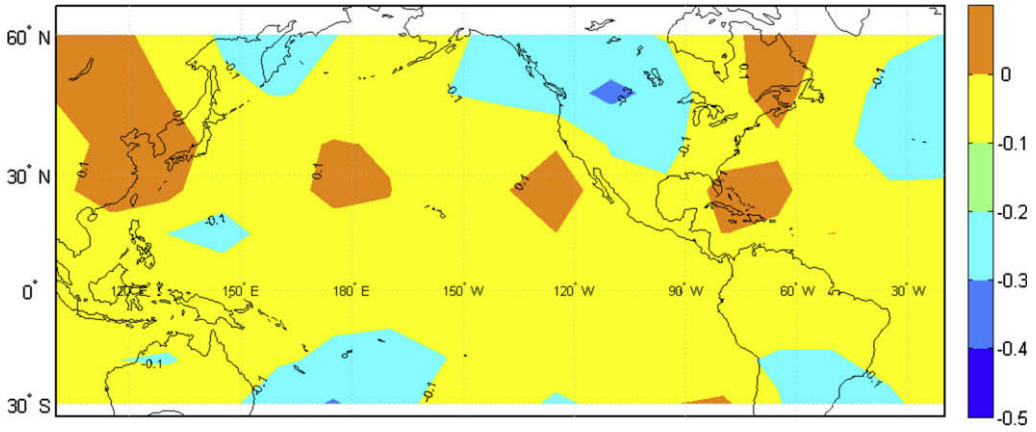

Fig. 4. Heterogeneous correlation map showing significant [$|r| > 0.21$ for 90% ($p < 0.1$) significance threshold] Z_{500} regions as related to NPRB streamflow stations for OND(-1) three month lead-time.

playing the highest significance. The region off the coast of Africa is similar to a region found in Tootle and Piechota (2006). These findings reinforce the stronger correlation of the AMO index.

The significant region for Z_{500} (northwest/north central US) was similar to the location found by Grantz et al. (2005). There is a long history of the relationship between SSTs and streamflow forecasting but Grantz et al. (2005) and the work presented here examined the outcome of incorporating the 500 mbar geopotential height. Z_{500} is approximately 18,000 feet above sea level and has been linked to various climate processes. In mid-latitudes, Z_{500} transitions rapidly from large to low values across a circumpolar jet stream. A jet stream (fast flowing narrow currents of air) is located where the geopotential height contours are closest together (changing in height most rapidly). This jet stream consists of a series of transient troughs and ridges, which are the upper air counterparts of surface cyclones and anticyclones. The relatively shorter wave troughs in the jet stream are usually associated with surface cyclones and precipitation. Especially in winter, precipitation is strongly modulated by Z_{500}, and the deeper the short-wave trough or the stronger the jet, the more intense the surface cyclone and the heavier the precipitation. The precipitation is concentrated in frontal disturbances located just downstream of a Z_{500} trough. In the NPRB, most of that precipitation in winter falls as snow on the mountain ranges flanking the south and west sides of the upper NPRB. The general pattern of the polar jet stream over the United States in winter is such that it comes down from the coast of Alaska, just south of Anchorage, and then moves laterally from northwest to southeast across the northern tier of the continental United States. For regions that are typically equatorward of the jet, such as California and possibly also the upper NPRB, an anomalous southward excursion of the jet on average, over the course of a winter, should imply more trough passages and thus more precipitation. Places typically poleward of the jet, such as Fairbanks, Alaska, tend to be wetter when the jet is anomalously far north, i.e. when Z_{500} is anomalously high (Geerts, personal communication, 3/10/2008). Grantz et al. (2005) explained that the Z_{500} and the wind vectors associated with the Z_{500} troughs and ridges drive winter precipitation over west central Nevada. These findings suggest that the winter weather in the west central US is predominately driven by the location and magnitude of wind vectors (i.e., jet streams). Meteorological analyses examining the relationship between the jet stream, and pressure troughs and ridges suggest that precipitation responds immediately to Z_{500}. The jet stream and its wave train are very transient (e.g., a trough and its associated frontal precipitation may pass an area in less than a day). (Geerts, personal communication, 3/10/2008). This concept of immediate response raises the question of how geopotential height index values can be incorporated into long lead-time forecasts.

The results of this study as well as those of Grantz et al. (2005) imply that an improved skill of streamflow forecasting is achieved at shorter lead-times. Since precipitation is an immediate response to geopotential heights it seems logical to conclude that there is no lag time between precipitation and the geopotential height index. Rather the geopotential heights are responsible for wintertime precipitation (falling as snow in the NPRB) when it is actually occurring (ONDJFM) and the three month lead-time is actually the typical time between when the snowfalls and the snow melts. We see a strong skill associated with the forecast utilizing OND(-1) geopotential heights because during those months the 500 mbar geopotential height index values are immediately driving the snowfall which settles, compacts, and then begins melting several months later and is the prominent source of streamflow volume. Similar logic can be applied to the JAS(-1) time period. In mountainous regions, some precipitation may fall as snowfall but a substantial portion may still be falling in the form of rain due to the warmer temperatures of July, August, and September. Due to the precipitation falling as rain and not snow, it is not accumulating as snowpack (which melts several months later and contributes to AMJJ streamflow) and therefore is not recognized as a skillful predictor in the model. Another question might be raised as to why not just use the actual snowpack amounts as measured at snow telemetry sites as opposed to incorporating Z_{500}.

The Natural Resource Conservation Service (NRCS) currently operates SNOTEL (snow water equivalent telemetry sites) throughout the west. However, January 1st data is only available back into the mid 1980's when most sites transferred from snow-course sites to automated telemetry sites. Prior to the mid 1980's actual snowpack depth was only available for the months of March, April and May. The work of Moser et al. (2009) concludes a strong correlation between streamflow and snow water equivalent recorded by SNOTEL sites in the NPRB mountainous headwater regions. The results of this study suggest that Z_{500} index values can be a skillful predictor of winter precipitation and thus spring streamflow, especially in mountainous NBRB regions where the precipitation falls as snow. Therefore, if the 500 mbar geopotential height index values can be used as predictors of snowfall it can be concluded that for the NPRB this snowfall would result in AMJJ streamflow volumes.

Conclusion

A method for developing spatial–temporal relationships between large scale oceanic–atmospheric influences and

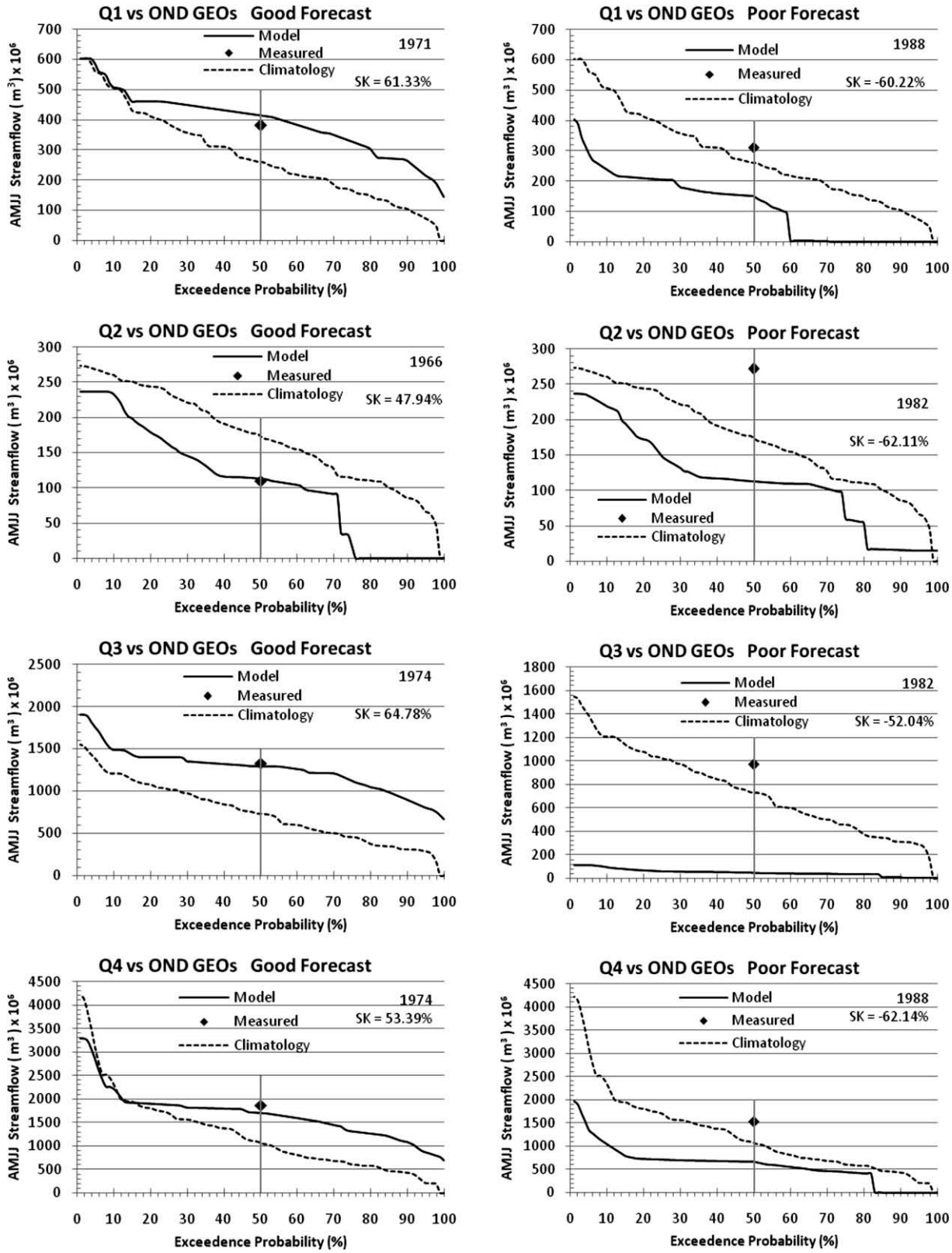

Fig. 5. Examples of poor and good forecasts for OND Z_{500} index values and individual streamflow stations.

incorporating those relationships into the development of exceedance probability forecasts for the North Platte River was performed. The North Platte River Basin is in a challenging location in terms of predefined climate index signals. The correlation between North Platte River streamflow volumes and the predefined Niño 3.4, PDO and AMO climate indices were found, in general, to be insignificant, thus creating the need to locate significant regions of oceanic–atmospheric variability. SVD was used to identify significant

(>90%) spatial–temporal regions of SST and Z_{500} such that temporal expansion series (1st mode) found could be used to generate exceedance probability forecasts. Due to the continuous nature of the exceedance probability forecast, it is especially useful because it allows the forecast user to assess the forecasted amount of streamflow at different levels of risk. The forecast model was applied at two lead-times, three month – OND(-1) and six month – JAS(-1). The results of the modeling process reveal that SSTs are a skillful six month lead-time predictor whereas Z_{500} produce more skillful three month lead-time forecasts. Various years were selected to provide examples of good (high cross-validated LEPS skill score) and poor forecasts. Over the 57 years used in this analysis, more good forecasts were developed versus poor forecasts, thus indicating that large scale oceanic–atmospheric climate variability is applicable to generating skillful long lead-time forecasts. The significant contribution of this work was the application of singular value decomposition techniques to identify predictors to be utilized in long lead-time streamflow forecasting models.

Acknowledgements

This research is sponsored by the Wyoming Water Development Commission, the USGS/State of Wyoming Water Research Program and the University of Wyoming, Office of Water Programs. The research at UNLV is supported by the National Science Foundation under award CMS-0239334, and the National Oceanic and Atmospheric Administration under award NA070AR4310228. The authors wish to thank Dr. Bart Geerts (University of Wyoming, Department of Atmospheric Sciences) for his assistance.

References

Blackmon, M.L., 1976. A climatological spectral study of the 500 mb geopotential height of the northern hemisphere. Journal of the Atmospheric Sciences 33, 1607–1623.

Blackmon, M.L., Wallace, J.M., Lau, N.C., Mullen, S.L., 1977. An observational study of the northern hemisphere wintertime circulation. Journal of the Atmospheric Sciences 34, 1040–1053.

Bretherton, C.S., Smith, C., Wallace, J.M., 1992. An intercomparison of methods for finding coupled patterns in climate data. Journal of Climate 5, 541–560.

Cayan, D.R., Peterson, D.H., 1989. The influence of North Pacific atmospheric circulation on streamflow in the west. In: Aspects of Climate Variability in the Pacific and the Western Americas. Geophysical Monograph Series, vol. 55. American Geophysical Union, pp. 375–397.

Cayan, D.R., Webb, R.H., 1992. El Niño/Southern Oscillation and streamflow in the western United States. El Niño: Historical and Paleoclimatic Aspects of the Southern Oscillation. Cambridge University Press, New York.

Elsner, J.B., Schmertmann, C.P., 1994. Assessing forecast skill through cross validation. Weather and Forecasting. 9, 619–624.

Enfield, D.B., Mestas-Nuñez, A.M., Trimble, P.J., 2001. The Atlantic multidecadal oscillation and its relation to rainfall and river flows in the continental US. Geophysical Research Letters 28 (10), 2077–2080.

Geerts, B., personal communication. Associate Professor in the Department of Atmospheric Sciences at the University of Wyoming.

Grantz, K., Rajagopalan, B., Clark, M., Zagona, E., 2005. A technique for incorporating large-scale climate information in basin-scale ensemble streamflow forecasts. Water Resources Research 41, W10410.

Hare, S., Mantua, N., 2000. Empirical evidence for North Pacific regime shifts in 1977 and 1989. Progress in Oceanography 47, 103–145.

Hunter, T., Tootle, G., Piechota, T., 2006. Oceanic–atmospheric variability and western US snowfall. Geophysical Research Letters 33, L13706. doi:10.1029/2006GL026600.

Kahya, E., Dracup, J.A., 1993. US streamflow patterns in relation to the El Niño/southern oscillation. Water Resources Research 29 (8), 2491–2503.

Kahya, E., Dracup, J.A., 1994a. The influences of Type 1 El Niño and La Niña Events on streamflows in the Pacific Southwest of the United States. Journal of Climate 7 (6), 965–976.

Kahya, E., Dracup, J.A., 1994b. The relationships between US streamflow and La Niña events. Water Resources Research 30 (7), 2133–2141.

Kalnay, E. et al., 1996. The NCEP/NCAR reanalysis 40-year project. Bulletin of the American Meteorological Society 77, 437–471.

Lall, U., 1995. Recent advances in non-parametric function estimation; Hydrologic applications, US Natl. Rep. Int. Union Geod. Geophys. 1991–1994. Reviews of Geophysics 33, 1093–1102.

Lall, U., Sharma, A., 1996. A nearest neighbor bootstrap for resampling hydrologic time series. Water Resources Research 32, 679–693.

Mantua, N.J., Hare, S.R., 2002. The Pacific decadal oscillation. Journal of Oceanography 59 (1), 35–44.

Mantua, N.J., Hare, S.R., Zhang, Y., Wallace, J.M., Francis, R.C., 1997. A Pacific interdecadal climate oscillation with impacts on salmon production. Bulletin of the American Meteorological Society 78, 1069–1079.

Maurer, E.P., Lettenmaier, D.P., Mantua, N.J., 2004. Variability and potential sources of predictability of North American runoff. Water Resources Research 40 (12), W09306.

McCabe, G.J., Palecki, M.A., Betancourt, J.L., 2004. Pacific and Atlantic Ocean influences on multidecadal drought frequency in the United States. PNAS 101 (12), 4136–4141.

Michaelsen, J., 1987. Cross-validation in statistical climate forecast models. Journal of Climate and Applied Meteorology 26, 1589–1600.

Moser, C., Soukup, T., Tootle, G., Piechota, T., Wulff, S., 2009. Incorporating antecendent soil moisture into streamflow forecasting. Journal of the American Water Resources Association, submitted for publication.

Newman, M., Sardeshmukh, P.D., 1995. A caveat concerning singular value decomposition. Journal of Climate 8, 352–360.

North Platte River Basin (Overview) HUC# 101800, 2008. Wyoming State Water Plan. <http://waterplan.state.wy.us/sdi/NP/NP-over.html>(Retrieved 21.03.08.).

Natural Resources Conservation Service, 2008. Water supply forecasting, a short primer. <http://www.wcc.nrcs.usda.gov/factpub/wsf_primer.html> (retrieved 15.01.08).

Philander, S.G., 1990. El Niño, La Niña and the Southern Oscillation. Academic Press, Inc., San Diego, CA.

Piechota, T.C., Dracup, J.A., 1999. Long range streamflow forecasting using El Niño-southern oscillation indicators. Journal of Hydrologic Engineering 4 (2), 144–151.

Piechota, T.C., Dracup, J.A., Chiew, F.H.S., McMahon, T.A., 1998. seasonal streamflow forecasting in Eastern Australia and the El Niño–southern oscillation. Journal of Water Resources Research 34 (11), 3035–3044.

Piechota, T.C., Chiew, F.H.S., Dracup, J.A., McMahon, T.A., 2001. Development of exceedance probability streamflow forecast. Journal of Hydrologic Engineering 6 (1), 20–28.

Potts, J.M., Folland, C.K., Jolliffe, I.T., Sexton, D., 1996. Revised "LEPS" scores for assessing climate model simulations and long-range forecasts. Journal of Climate 9, 34–53.

Rajagopalan, B., Lall, U., 1999. A *k*-nearest-neighbor simulator for daily precipitation and other weather variables. Water Resources Research 35, 3089–3101.

Rajagopalan, B., Cook, E., Lall, U., Ray, B.K., 2000. Spatiotemporal variability of ENSO and SST teleconnections to summer drought over the United States during the twentieth century. Journal of Climate 13, 4244–4255.

Rogers, J.C., Coleman, J.S.M., 2003. Interactions between the Atlantic multidecadal oscillation, El Niño/La Niña, and the PNA in winter Mississippi Valley stream flow. Geophysical Research Letters 30 (10), 1–4. 25.

Serreze, M.C., Clark, M.P., McGinnis, D.L., Robinson, D.A., 1998. Characteristics of snowfall over the eastern half of the United States and relationships with principal modes of low-frequency atmospheric variability. Journal of Climate 11, 234–250.

Shabbar, A., Skinner, W., 2004. Summer drought patterns in Canada and the relationship to global sea surface temperatures. Journal of Climate 17, 2866–2880.

Silverman, B.W., 1986. Density Estimation for Statistics and Data Analysis. Chapman and Hall, New York.

Smith, T.M., Reynolds, R.W., 2003. Extended reconstruction of global sea surface temperatures based on COADS data (1854–1997). Journal of Climate 16, 1495–1510.

Smith, T.M., Reynolds, R.W., 2004. Improved extended reconstruction of SST (1854–1997). Journal of Climate 17, 2466–2477.

Souza Filho, F.A., Lall, U., 2003. Seasonal to interannual ensemble streamflow forecasts for Ceara, Brazil: applications of multivariate, semiparametric algorithm. Water Resources Research 39 (11), 1307. doi:10.1029/2002/WR001373.

Tootle, G.A., Piechota, T.C., 2004. Suwannee river long-range streamflow forecasts based on seasonal climate predictors. Journal of the American Water Resources Association 40 (2), 523–532.

Tootle, G.A., Piechota, T.C., 2006. Relationships between Pacific and Atlantic ocean sea surface temperatures and US streamflow variability. Water Resources Research 42, W07411.

Tootle, G.A., Piechota, T.C., Singh, A., 2005. Coupled oceanic–atmospheric variability and US streamflow. Water Resources Research 41, W12408. doi:10.1029/2005WR004381.

Tootle, G.A., Piechota, T.C., Gutierrez, F., 2008. The relationships between pacific and Atlantic ocean sea surface temperatures and Colombian streamflow variability. Journal of Hydrology 349 (3–4), 268–276.

Trenberth, K.E., 1997. The definition of El Niño. Bulletin of the American Meteorological Society 78, 2271–2777.

United States Geological Survey, 2007. USGS Real-Time Water Data for USA. National Water Information System. <http://waterdata.usgs.gov/nwis/rt?> (retrieved 17.11.07).

Uvo, C.B., Repelli, C.A., Zebiak, S.E., Kushnir, Y., 1998. The relationships between tropical Pacific and Atlantic SST and northeast Brazil monthly precipitation. Journal of Climate 11, 551–562.

Wallace, J.M., Gutzler, D.S., Bretheron, C.S., 1992. Singular value decomposition of wintertime sea surface temperature and 500-mb height anomalies. Journal of Climate 5, 561–576.

Wang, H., Ting, M., 2000. Covariabilities of winter precipitation and Pacific sea surface temperatures. Journal of Climate 13, 3711–3719.

Ward, N.M., Folland, K.K., 1991. Prediction of seasonal rainfall in the North Nordeste of Brazil using Eigenvectors of sea-surface temperature. International Journal of Climatology 11, 711–743.

Xoplaki, E., Luterbacher, J., Burkard, R., Patrikas, I., Maheras, P., 2000. Connection between the large-scale 500 hPa geopotential height fields and precipitation over Greece during wintertime. Climate Research 14, 129–146.